Title

Haploinsufficiency of the mouse *Tshz3* gene leads to kidney dysfunction

Authors

Irene Sanchez-Martin[1], Pedro Magalhães[2], Ahmed Fatmi[1], Fabrice Richard[1], Thien Phong Vu Manh[3], Andy Saurin[1], Guylène Feuillet[4,5], Colette Denis[4,5], Joost P. Schanstra[4,5], Petra Zürbig[2], Xavier Caubit[1], Laurent Fasano[1,*]

Affiliation

1 Aix Marseille Univ, CNRS, IBDM, UMR7288, Marseille, France

2 Mosaiques Diagnostics GmbH, Hannover, Germany.

3 Aix Marseille Univ, CNRS, INSERM, CIML, Centre d'Immunologie de Marseille-Luminy, Marseille, France.

4 Institut National de la Santé et de la Recherche Médicale (INSERM), U1297, Institut of Cardiovascular and Metabolic Disease, Toulouse, France.

5 Université Toulouse III Paul-Sabatier, Toulouse, France.

*** Correspondence:**

Correspondence should be addressed to Laurent Fasano

laurent.fasano@univ-amu.fr

Abstract

Renal tract defects and autism spectrum disorder (ASD) deficits represent the phenotypic core of the 19q12 deletion syndrome caused by the loss of one copy of the *TSHZ3* gene. While a proportion of *Tshz3* heterozygous (*Tshz3*$^{+/lacZ}$) mice display ureteral defects, no kidney defects have been reported in these mice. The purpose of this study was to characterize the expression of *Tshz3* in adult kidney as well as the renal physiological consequences of embryonic haploinsufficiency of *Tshz3* by analyzing the morphology

and function of *Tshz3* heterozygous adult kidney. Here, we described *Tshz3* expression in the smooth muscle and stromal cells lining the renal pelvis, the papilla and glomerular endothelial cells (GEnCs) of the adult kidney. Histological analysis showed that *Tshz3*$^{+/lacZ}$ adult kidney had an average of 29% fewer glomeruli than wild type kidney. Transmission electron microscopy (TEM) of *Tshz3*$^{+/lacZ}$ glomeruli revealed ultrastructural defects. Compared to wild type, *Tshz3*$^{+/lacZ}$ mice showed no difference in their urine parameters but lower blood urea, phosphates, magnesium and potassium at 2 months of age. At the molecular level, transcriptome analysis identified differentially expressed genes related to inflammatory processes in *Tshz3*$^{+/lacZ}$ compare to wild type (WT; control) adult kidneys. Lastly, analysis of the urinary peptidome revealed 33 peptides associated with *Tshz3*$^{+/lacZ}$ adult mice. These results provide the first evidence that in the mouse *Tshz3* haploinsufficiency leads to cellular, molecular and functional abnormalities in the adult mouse kidney.

Introduction

Congenital anomalies of the kidneys and urinary tract (CAKUT) are the most common cause of renal failure in children [1]. Ureteropelvic junction obstruction (UPJO), the most common paediatric renal obstructive disorder, has an incidence of 1 in 1000-1500 live births screened by antenatal ultrasound [2]. Congenital UPJO is usually caused by the presence of an aperistaltic segment of the ureter, preventing the efficient transport of the urine from the kidney to the bladder. UPJO can result from the decrease in the number of smooth muscle cells, interstitial Cajal-like cells and nerve fibers in the ureteropelvic junction. Therefore, impaired transport of urine can lead to an increase in back-pressure on the kidney, hydronephrosis, and progressive damage to the kidney function [3].

The *TSHZ3* gene (Teashirt zinc-finger homeobox family member 3; also known as ZNF537), which encodes a zinc-finger transcription factor, was recently identified as the critical region for a 19q12 deletion syndrome (19q12DS): patients with *TSHZ3* heterozygous deletion show lower (i.e. vesicoureteral reflux grade 2) and upper (i.e. UPJO) urinary tract defects as well as kidney (i.e. hydronephrosis and nephrolithiasis) defects[4].

Tshz3 homozygous mutant mice (*Tshz3*$^{lacZ/lacZ}$) have been used to explore the pathogenesis of *Tshz3* in UPJO [5,6]. Studies have shown that from embryonic day (E) 12.5 onwards TSHZ3 positive cells are detected in the mouse ureter and the kidney [5]. In the

embryo, *Tshz3* plays a key role in smooth muscle differentiation by regulating *Myocardin (myocd)* expression and MYOCD activity [5,6]. *Tshz3*$^{lacZ/lacZ}$ mutant mice die perinatally because of their inability to breathe and display bilateral UPJO and hydronephrosis [5,7]. In comparison, one-fourth of *Tshz3*$^{+/lacZ}$ heterozygous embryos display a unilateral UPJO and hydronephrosis and about 50% die at birth [5-7]. However, the impact of *Tshz3* haploinsufficiency on the postnatal kidneys has never been investigated so far.

Therefore, the main aim of this study was to determine whether *Tshz3* heterozygote mice exhibit kidney defects in order to gain insights on whether haploinsufficiency may help explaining kidney diseases reported in patients with heterozygous deletion of *TSHZ3*.

Results

TSHZ3 expression in adult kidneys.

Previous analyses performed during development indicate that the temporal and spatial distribution of β-galactosidase (ß-gal) protein in *Tshz3*$^{+/lacZ}$ mice faithfully reproduces the expression of *Tshz3*/TSHZ3 [5,6]. Here we used the same approach to characterize the expression of *Tshz3*/TSHZ3 in sections of *Tshz3*$^{+/lacZ}$ adult kidneys. X-Gal staining performed on *Tshz3*$^{+/lacZ}$ adult kidney revealed that *Tshz3* is expressed in the pelvic region and ureter, the papilla, perivascular region and the glomeruli (**Fig. 1A-F**). To further characterize the expression of TSHZ3 in the glomeruli, we performed immunostaining, using glomerular cells markers. These analyses showed that β-gal positive cells were endothelial cell (CD31-positive) but not podocytes (Dachshund 1 positive) or mesangial cells (NG2 positive) (**Fig. 1G-I**). Double immunostaining for β-gal and Smooth muscle alpha-actin (SMAA) confirmed the expression of TSHZ3 in smooth muscle cells in the pelvic region and in SMA-negative Dachshund 1-positive stromal cells lining the urothelium (**Fig. 2**).

Tshz3$^{+/lacZ}$ mice showed glomerular defects.

Comparison of 8-week-old adult kidney histology revealed a decrease of 28.8% in glomerular density in *Tshz3*$^{+/lacZ}$ compared to WT (**Fig. 3A, B and supplementary Fig. 4**). The same analysis performed with 40-week-old adult kidneys revealed a 44.2% reduction of glomerular density in *Tshz3*$^{+/lacZ}$ *vs.* WT. In order to identify glomerular

91 morphological changes in *Tshz3*$^{+/lacZ}$ mice, we conducted an ultrastructural analysis using
92 transmission electron microscopy (TEM). While this analysis did not identify a
93 significant variation of the proportion of the size of the fenestration and endothelial layer
94 (**Fig. 3C, D**), it revealed a significant reduction of the thickness of the glomerular
95 basement membrane (GBM) in glomeruli of *Tshz3*$^{+/lacZ}$ mutants (144.2 ± 4.2 nm)
96 compared to WT (155.1 ± 3.32 nm) (**Fig. 3E, F**). TEM analysis also showed a
97 significantly increased foot process width (351.7 ± 5.03 nm) in *Tshz3*$^{+/lacZ}$ compared to
98 WT (303.4 ± 6.57 nm) podocytes, suggesting foot process effacement (FPE) (**Fig. 3G,**
99 **H**).

100 **Blood electrolytes are modified in *Tshz3*$^{+/lacZ}$ mice.**

101 To characterize the effects of *Tshz3* haploinsufficiency on kidney filtration, we performed
102 biochemical measurements on blood samples and generated biochemical profiles for
103 *Tshz3*$^{+/lacZ}$ and WT adult mice tested at 58-64 days-of-age. While this analysis
104 demonstrated that *Tshz3*$^{+/lacZ}$ mice had no proteinuria compared to WT, it showed a
105 significant reduction of the urea ($P<0.013$), phosphates ($P<0.011$), magnesium ($P<0.014$),
106 potassium ($P<0.0034$) as well as an increased concentration of sodium ($P<0.012$) (**Fig.**
107 **4; Table 1a**). This analysis also suggested a trend for an increased concentration of
108 creatinine in *Tshz3*$^{+/lacZ}$ compared to WT (15.91 ± 1.51 vs. 12.36 ± 2.07 µm/l), but no
109 statistical significance was observed.

110

111 **The *Tshz3*$^{+/lacZ}$ adult kidney showed differential expression of genes involved in**
112 **inflammatory processes.**

113 To identify *Tshz3*-regulated genes in the adult kidney, RNA sequencing analysis was
114 performed with samples extracted from *Tshz3*$^{+/lacZ}$ (n=6) and wild type (WT; controls,
115 n=6) adult mouse kidneys. 97 differentially expressed genes (DEGs) were identified,

among which 55 were up-regulated and 42 were down-regulated (adjusted p-value < 0.01) (**Table 1b**). Thereafter, we sought to take advantage of the single-cell transcriptome of mouse glomeruli [8] and adult kidney[9] to identify the cell types in wild type kidneys that expressed the genes differentially expressed in *Tshz3*$^{+/lacZ}$ kidney. This analysis identified 58 genes expressed in podocytes, 31 in mesangial cells, 27 in immune cells, 40 in tubules and 43 in GECs, which might be direct targets of TSHZ3 (**Table 1c**). We also found that some DEGs were shown to be markers of proximal tubules (*Aspdh*, *Snhg11* and *D630029K05Rik*, a long non-coding RNA) or myeloid lineage (*Cd74*, *Gusb*, *H2-Aa*, *H2-Ab1*, *Lyz2*, *Mpeg1* and *Vcam1*), including macrophages and dendritic cells [10].

To characterize the differential expression data and to identify biological changes that occur in *Tshz3*$^{+/lacZ}$ kidneys, we performed different enrichment analyses. As only a few genes showed very strong differential expression, we applied gene set enrichment analysis (GSEA [11,12]) using a ranked gene list. We chose the updated public genesets available on MSigDB [12] and identified positive enrichment in the kidneys of *Tshz3*$^{+/lacZ}$ adult mice for gene sets related to "interferon-gamma response", "epithelial to mesenchymal transition", "inflammatory response" and negative enrichment for genes related to "Oxidative Phosphorylation" and "Xenobiotic Metabolism" (**Table 1d; Supplementary Fig. 1**). Furthermore, ingenuity pathway analysis (IPA) of the DEGs revealed enrichment of cellular processes centered on inflammatory and kidney diseases (**Supplementary Fig. 2A, B**). This analysis showed that the relevant toxicity phenotypes and pathology endpoints associated with the DEGs in *Tshz3*$^{+/lacZ}$ mice were centered on the kidney and identified interferon-gamma (IFNG) as an upstream regulator (**Supplementary Fig. 2B, C**). Moreover, enrichment analysis of pathways and transcription factor using enrichR [13] also identified the "*interferon gamma*" pathway but

also "*collagen formation*" and "*extracellular matrix organization*" as significantly enriched in *Tshz3*$^{+/lacZ}$ adult kidneys (**Table 1e**). Interestingly, the ChIP enrichment analysis (ChEA) and a database search revealed that 22 DEGs (21.68%) are direct targets of the transcription factor interferon regulatory factor 8 (IRF8) (**Table 1f**).

Using RT-qPCR we confirmed the DEG status observed by RNA-seq analysis for *Ciita, Pld4* (two targets of IRF8), *Tlr7* (IRF8 target that promotes IFNG production [14]) and the proinflammatory *Npy* (**Supplementary Fig. 3**).

Genes differentially expressed in *Tshz3*$^{+/lacZ}$ adult kidney are associated with ASD

To gain insights into *TSHZ3* function, we studied the disease association of the 80 non-ambiguous human orthologs of the mouse DEGs (**Table 1g**). This analysis identified 35/80 genes (43.75%), which were established or putative causes for kidney disorders. Interestingly, 8 of these genes have been also associated with ASD (**Table 1h**).

Identification of *Tshz3*$^{+/LacZ}$-related urinary peptides

Since *Tshz3*$^{+/lacZ}$ mice exhibit dysregulated kidney expression of several genes and altered hematological parameters, we sought to analyze their urinary peptidome. Urine samples derived from *Tshz3*$^{+/LacZ}$ (n=15) and WT (n=12) were analyzed by capillary electrophoresis coupled to mass spectrometry (CE-MS). Comparison of urinary peptidome profiles led to the identification of 33 peptides that were significantly (adjusted p-value < 0.05) associated with *Tshz3*$^{+/lacZ}$ (**Fig. 5**). Protein fragments from clusterin (CLUS), complement factor D (CFAD), histone H2B type 1-F/J/L (H2B1F), major urinary protein 17 (MUP17), tripeptidyl-peptidase 1 (TPP1) and uromodulin (UMOD), as well as a large number (27) of collagen fragments, were identified (**Table 1i)**. *Tshz3*$^{+/lacZ}$ mice showed a decreased concentration of uromodulin and an increased concentration of peptides from clusterin, complement factor D, histone H2B type 1-F/J/L,

major urinary protein 17 as well as tripeptidyl-peptidase 1 fragments. Twelve collagen peptides were in higher abundance and fifteen in lower abundance. As UPJO can lead to significant kidney damage, we compared the identified 33 urinary peptides from mice with those of the CKD273 classifier, a predictive marker of chronic kidney disease (CKD) progression in humans[15]. This analysis identified 14 similar (orthologs) human peptides in the CKD273 classifier, most of which were collagen fragments (10 from collagen type I alpha-1 chain and 3 from type III alpha-1 chain). One peptide fragment was from uromodulin.

Discussion

Previously, we reported that in mice and humans, haploinsufficiency of *Tshz3/TSHZ3* results in hydroureter [5,16] and that individuals with *TSHZ3* heterozygous deletion are at risk to develop kidney diseases [16]. However, the expression of *Tshz3* in adult kidney and the morphology of *Tshz3* heterozygous adult kidney have not been investigated before. Herein, we characterized TSHZ3 expression in the adult mouse kidney, in particular in glomeruli where TSHZ3 is specifically expressed in endothelial cells (GEnCs), which is supported by single-cell RNA sequencing analysis [8]. Using $Tshz3^{+/lacZ}$ heterozygous mice, we have also uncovered a key role for the TSHZ3 transcription factor in controlling the glomerular density and morphology. Notably, we showed that $Tshz3^{+/lacZ}$ mice have abnormal blood electrolytes and identified $Tshz3^{+/LacZ}$-related urinary peptides. In addition, by coupling transcriptomics with *in silico* analysis, we showed that in kidneys from $Tshz3^{+/LacZ}$ mice, the expression of genes associated with inflammatory processes and of renal- and ASD-associated was different from that in WT mice. Combined with our previous reports, our data suggest that the *Tshz3* heterozygous mice constitute a model that replicates many of the corresponding human disease phenotypes.

The GEnCs, together with the glomerular basement membrane (GBM) and the podocytes, constitute the glomerular filtration barrier (GFB), which selectively filtrates the plasma. The GBM derives from the fusion of the basement membranes of both GEnCs and podocytes, and in adult kidney, the GEnCs may contribute to the renewed biosynthesis of the GBM. Because abnormalities in each of the three constituents of the GFB can lead to proteinuria and kidney disease, TEM was used to assess fine structures of the GFB. While TEM analysis revealed no obvious structural phenotype in TSHZ3-expressing GEnCs, it provided evidence that *Tshz3* haploinsufficiency leads to GBM thinning and change in podocyte morphology evidenced by foot process effacement (FPE). Interestingly, individuals with a thin GBM have hematuria but minimal proteinuria [17] and, accordingly, we found that the thin GBM as well as the defects in the podocytes did not result in the development of proteinuria. In future research it would be interesting to investigate whether these defects are associated with hematuria. At present, the primary cause of the structural defects observed in the GBM and the podocytes remains unknown. However, since communication between intraglomerular cells is required for proper development and maintenance of the GFB [18], GBM thinning and foot process effacement might be the direct or indirect consequences of an abnormal cross-talk between the TSHZ3-positive GEnCs and other glomerular cells. Furthermore, *Tshz3* may be transiently expressed in glomerular cell lineages. Nevertheless, the comparison of the urinary peptidome of $Tshz3^{+/lacZ}$ and WT adult led to the identification of 27 collagen and 6 non-collagen peptides associated with $Tshz3^{+/lacZ}$ mice. Among the collagen fragments displaying a deregulation (e.g. 12 increased or 15 decreased), we identified thirteen collagen fragments that overlap the CKD273 classifier that might be indicative of the development of fibrosis [19,20]. As previously suggested [21], the fragments overlapping the human CKD273 classifier could be used as biomarkers to assess renal function in patients

with *TSHZ3* heterozygous deletion. Interestingly, our analysis of urinary peptides also revealed an under-representation of a MUP17 peptide in *Tshz3*$^{+/lacZ}$ mice. The MUP17 protein is predominantly expressed in males and dominant males significantly increased the secretion of MUP17 in social conditions [22,23]. In the future, it would be interesting to study the relationship between variations in the level of MUP17 and the severity of the social behavior deficit observed in *Tshz3*$^{+/lacZ}$ mice. To further evaluate renal function, we performed biochemical measurements on blood samples and generated biochemistry profiles. This analysis identified a significantly reduced concentration for urea, phosphates, magnesium and potassium in *Tshz3*$^{+/lacZ}$ mice. Reduced serum urea is less frequent and usually of less clinical significance than increased serum urea [24,25]. Nevertheless, overhydration is one of the rare causes of decreased serum urea and we routinely observed that *Tshz3*$^{+/lacZ}$ mice drink more and urinate more than WT mice (not shown). The lower plasma magnesium (hypomagnesaemia), phosphate (hypophosphatemia) and potassium (hypokalemia) serum concentration are associated with defective reabsorption/excretion process in the distal nephron [26-28]. Interestingly, single-cell transcriptional profiling of the healthy mouse kidney showed expression of *Tshz3* in the proximal tubule, distal convoluted tubule as well as in collecting duct principal and intercalated cells [9], suggesting that *Tshz3* haploinsufficiency might impact different components of the nephron. In the future, these transcriptomic data should be complemented by a comparative analysis of the expression of TSHZ3 and segment-specific tubular markers in WT and *Tshz3*$^{+/lacZ}$ adult kidneys. To identify pathways that might be altered, we performed RNA-seq analysis and detected 48 statistically significant changes in gene expression in adult kidneys of *Tshz3*$^{+/lacZ}$ as compared to WT. Based on the results of enrichment analyses, we detected the involvement of inflammation-related pathways such as interferon-gamma. Of note, seven DEGs (*Crym, Ctss*, *Fasn*, *Fcgrt,*

243 *Gabrb3, Lyz2*, and *Vcam1*) were found to be associated with kidney diseases, including
244 renal inflammation, crescentic glomerulonephritis or end-stage renal failure.
245 Interestingly, population-based studies support that autism spectrum disorder (ASD) and
246 kidney disease coexist in several genetic disorders (for review see Table 2 in [29]),
247 suggesting that the same genetic modification can affect neurodevelopment and
248 nephrogenesis. However, because the genetic alterations (deletion or duplication)
249 associated with these disorders often encompass several genes, it is still unclear how these
250 genes contribute to the underlying molecular mechanisms. In this context, the *TSHZ3*
251 gene which associates ASD with a congenital kidney condition is quite unique[4] and our
252 findings that heterozygous deletion of *Tshz3* alters some of the key functions performed
253 by the kidneys might be relevant for patients with *TSHZ3* heterozygous deletion. Indeed,
254 we previously reported heterozygous deletion of the *TSHZ3* gene in six patients with renal
255 tract defects, including one with nephrolithiasis and a second one with postnatal
256 echogenic kidney and low glomerular filtration rate (Table1 in [4]) who required renal
257 transplant (Table 2 in [30]). These results might also provide to be of interest for cognitive
258 defects link to TSHZ3 haploinsufficiency. For now, the role of low plasma concentration
259 of magnesium in ASD is still a matter of debate. While two studies did not find a
260 statistically significant difference in levels of magnesium in children diagnosed ASD [31,32],
261 two other studies [33,34] demonstrated lower levels of magnesium in children diagnosed
262 with ASD. So far, *Tshz3* mouse models have been shown to be quite analogous to the
263 clinical problems (i.e. ASD-associated deficits, hydroureter and hydronephrosis) reported
264 in patients with *TSHZ3* heterozygous conditions [4,5]. Our results generate new hypotheses
265 that might lead to further understanding of the clinical problems and to a better diagnosis
266 management of *TSHZ3* patients.
267
268

Materials and methods

Mouse strain and genotype

The *Tshz3*$^{+/LacZ}$ mouse line has been described previously [5].

Samples collection and RNAseq

For RNA sequencing, *Tshz3*$^{+/LacZ}$ and wild-type mice kidneys were collected at 60 days-of-age. The mean values for body weight of the *Tshz3*$^{+/LacZ}$ and wild-type were 34.7± 3.9 g (n=6) and 34.6 ± 6.5 g (n=6), respectively. Dissected kidneys were stored in RNAlater solution (Qiagen) and kept frozen at -80 °C until RNA extraction.

Total individual kidney RNA was extracted using anRNeasy Maxi kit75162 Lot.260018727/ Lot.160012031 from Quiagen according to manufacturer's instructions. The integrity of RNA was assessed using a chip-based capillary electrophoresis machine and RNA concentration determined using a full spectrum (220-750nm) spectrophotometer. The quality control of the RNA was additionally checked with RNA 6000 Pico de Agilent Technologies, according to the manufacturer's instructions. To obtain two independent total RNA preparations from the two different conditions (wild type: WT1 & WT2; *Tshz3*$^{+/LacZ}$: HET1 & HET2) we pooled RNA from 3 kidneys per group in the same proportion. The starting material (1µg Total mRNA, dissolved in RNase-, DNase- and protease-free molecular grade water) was sent to GATC (Eurofins) for sequencing (Genome Sequencer Illumina HiSeq).

Sequences (fastq format) were mapped to the mm10 version of the mouse genome to generate Sequence Alignment/Map (SAM/BAM) format. After normalization, analysis of differentially expressed genes (DEGs) was performed using both the Bioconductor (http://www.bioconductor.org) package DESeq/DESeq2 and the package edgeR.

This analysis generated differential expression lists with False Discovery Rates (FDRs), which are derived from p-values corrected for multiple testing using the Benjamini-Hochberg method. 6 files in total were generated: FDR 1%, 10% for both UCSC (transcripts) and ENSEMBL (genes).

EnrichR tool [13] was used to performed enrichment analysis with “pathways”, gene ontology biological processes (GOBP) and transcription factor (ChIP Enrichment Analysis, ChEA). Gene set enrichment analysis (GSEA) was performed using the software provided by the Broad Institute [35,36] with default parameters and a pre-ranked

gene list calculated based on the10 negative $\log_{10}$ of the *P*-value from DESeq2 analysis multiplied by the sign of differential expression.

mRNA extraction, cDNA synthesis and quantitative real-time PCR (RT-qPCR)

Total RNA from adult kidneys of WT and *Tshz3*$^{+/lacZ}$ mice was prepared using a RNeasy Maxi Kit (ref 75162 Qiagen™), and first-strand cDNA was synthesized using a Maxima First Strand cDNA Synthesis Kit with dsDNase (ThermoFisher Scientific™ ref K1671 50). All samples from each experiment were reverse-transcribed at the same time, and real-time PCR was performed on a StepOne+ qPCR detection system (Applied Biosystems™) using Luminaris Color HiGreen High ROX qPCR Master Mix (Thermo Fisher Scientific™ ref K0362). RT-qPCR conditions were as follows: 40 cycles of 95 °C for 15 s and 60 °C for 60 s. Reactions were run in triplicate in three independent experiments. The geometric mean of the housekeeping gene GAPDH was used as an internal control to normalize variability in expression levels, and samples were also normalized to their respective control group. Specificity of reactions was verified by melt curve analysis. Primer sequences used for Sybr qPCR are as follows:

	gene	Primer FW	Primer Rev
1	*Gbp4*	CAGGCTCTACATGGACATGAGG	TGCCTGCAAGATGGAACTCTCG
2	*Ciita*	ACCTTCGTCAGACTGGCGTTGA	GCCATTGTATCACTCAAGGAGGC
3	*Tlr7*	GTGATGCTGTGTGGTTTGTCTGG	CCTTTGTGTGCTCCTGGACCTA
4	*Npy*	TACTCCGCTCTGCGACACTACA	GGCGTTTTCTGTGCTTTCCTTCA
5	*Gapdh*	GTCTCCTGCGACTTCAACAGCA	ACCACCCTGTTGCTGTAGCCGT

Expression data were normalized to controls and the variability in expression levels was analyzed using the $2^{-\Delta\Delta CT}$ method described Livak and Schmittgen [37].

Variables which showed a p-value less than 0.05 in the resulting model were considered to have a significant effect. These statistical analyses were performed by unpaired t-tests with the qbase+ software version 2 (Biogazelle).

Immunological and in situ hybridization analysis

Adult mice were transcardially perfused with phosphate-buffered saline (PBS, 10 mM, pH 7.4), followed by 4% paraformaldehyde (PFA) in PBS under ketamine (150 mg/kg) and xylazine (20 mg/kg) anesthesia. Kidneys were post-fixed in 4% paraformaldehyde

(PFA; EMS Lot.160401) for 2 h at 4 °C, cryoprotected with 30% sucrose solution in PBS and frozen (Iso-Pentane RPE524391 Carlo Erba at dry ice temperature). Immunostaining was performed on 12-µm cryosections from tissues embedded in OCT compound. Cryosections were washed with 0.2% Tween/PBS for 15 min and then blocked in 10% goat serum 0.1%/0.1% Tween/PBS for 1 h. Sections were incubated with primary antibodies overnight at 4 °C. Secondary antibodies were incubated 2 h at room temperature, and after several washes, sections were counterstained with DAPI for 10 minutes.

The following primary antibodies were used: anti-β-galactosidase (chicken, 1/1000, ab9361, Abcam; rabbit, 1/1000, Cappel), mouse anti-NG2 (1/100, MAB5384 Millipore), rabbit anti-CD31/Pecam (1/100 MEC13.3, BD Pharmingen) and rabbit anti-DACH11 (1/100, Proteintech 10914-1-AP). Secondary antibodies: Alexa-Fluor-546 goat anti-mouse; Alexa-Fluor-546 donkey anti-rabbit, Alexa-Fluor 488 donkey anti-mouse, Alexa-Fluor-488 donkey anti-chicken. Slides were mounted with Fluoromount-G, Southern Biotech Lot: B0216-N156. Images were acquired using a laser scanning confocal microscope (LSM780; Carl Zeiss) and processed using Adobe Photoshop.

For X-gal staining, kidneys/ureters were dissected from non-perfused animals, kidneys were cut in two according to the sagittal plane, and tissues were fixed for 1 h in 1% PFA. Detection of β-galactosidase activity was done on tissues or on 14-µm cryostat sections incubated in the dark in staining solution at 37 °C. X-gal staining was performed as described [38].

Samples were paraffinized after washing in increasing alcohol concentrations (70%, 80%, 90%, 97% and 100%) VWR chemicals for one day and finally with Xylene 33817 (Sigma-Aldrich) for 2 h, and immersed in paraffin Paraplast X-TRA from Sigma at 65 °C. Staining was performed with Hematoxylin (HHS32-1L Lot. 064K4354 Sigma-Aldrich), Eosin (Ht110230-1L Sigma-Aldrich), Trichrome Masson (Lot.17301-V04 Ral Diagnostics).

Transmission electronic microscopy and quantification

Kidneys were perfused as described above, rapidly dissected and postfixed in 2% PFA, 2.5% glutaraldehyde in cacodylate buffer (pH 7.2) overnight at 4 °C. The kidneys were put in 1% OsO_4 solution in cacodylate buffer for 1 h on ice, then dehydrated on ice and

362 embedded in resin (EPON 912). Sample were polymerized 48 h at 60 °C. Ultrathin
363 sections (80-nm) performed on Leica UCT were poststained with 2% uranyl acetate,
364 followed by Reynolds' lead citrate. Section were examined with a high-resolution
365 transmission electron microscope (Tecnai G2 (FEI), Netherland) at 200 kV and images
366 were acquired with a Veleta camera (Olympus). EM images were opened and analyzed
367 with ImageJ software [39]; the straight-line tool was used to measure GBM thickness and
368 endothelial cell fenestration on randomly selected electron micrographs. The same
369 approach was used for morphometric analysis of foot process effacement, as described
370 previously [40,41].
371
372 **Blood samples**
373 Blood samples were collected from *Tshz3*$^{+/LacZ}$ (n= 11; 5 females and 6 males) and WT
374 mice (n=11; 6 females and 5 males) at 60 days-of-age. The mean values for body weight
375 of *Tshz3*$^{+/LacZ}$ and wild-type were 38.27± 7.8 (n=11) and 33.01 ± 4.9 (n=11). Mice were
376 anaesthetized by an intraperitoneal injection of ketamine/xylazine (0.1 ml/10 g body
377 weight) prior to manipulation. Anesthesia was maintained by using 1.7% to 2.5%
378 isoflurane delivered in 600 ml/min oxygen and a closely fitting facemask. Blood was
379 collected by cardiocentesis puncture in heparinize tubes with EDTA and also in tubes
380 without anticoagulant, centrifuging at 4 ºC immediately after extraction. The total blood
381 volume in 30-40 g mice is approximately 2 to 3 ml. The maximum volume that could be
382 collected safely at a single survival time point was approximately 800-1000 µl. Blood
383 tests were outsourced to Laboklin G.m.b.H. and performed using a Siemens' high-volume
384 hematology analyzer (ADVIA 2120i) and a Roche' chemistry analyzer (Cobas 8000
385 c701).
386
387 **Urine samples**
388 Urine samples were collected from *Tshz3*$^{+/LacZ}$ (n= 7; 4 females and 3 males) and WT
389 mice (n=7; 6 females and 1 males) at 60 days-of-age.
390 Animals were placed in a clean, dry, empty, and transparent individual cage. A non-
391 absorbable plastic, fully sanitizable material was laid on the floor of the cage. During
392 urine collection, water bottles were provided but no food was given to limit contamination
393 with faeces or animal feed. The mouse was monitored all time and removed as soon as it
394 urinated. The voided urine was aspirated with a Gilson Pipetman and transfert to a 1.5
395 mL sterile microcentrifuge tube (kept on ice). Collected urine was stored at -80C prior to

396 analysis. Due to the small amount of urine collected, the procedure was repeated during
397 three consecutive days to obtain 300ul of urine for each mouse.
398
399 **Urinary Proteomics**
400 *Sample Preparation:* Urine samples were collected and frozen at -80°C as described
401 above. Immediately before preparation, mice urine samples were thawed on ice. 150 µl
402 of urine was mixed with a similar volume of a solution containing 2 M urea, 10 mM
403 NH_4OH, and 0.02% sodium dodecyl sulfate (SDS). To remove high molecular weight
404 molecules, samples were ultrafiltrated (3,400 × g for 45 min at 4°C) using a Centrisart
405 20kDa cut-off centrifugal filter device (Satorius, Göttingen, Germany) until 200 µl of
406 filtrate was obtained. Afterwards, the filtrate was desalted by a NAP5 gel filtration
407 column (GE Healthcare BioSciences, Uppsala, Sweden) to eliminate electrolytes and
408 urea, hence decreasing matrix effects. The samples were lyophilized in a Savant
409 SpeedVac SVC100H connected to a Virtis 3L Sentry freeze dryer (Fischer Scientific,
410 Illkirch, France), consequently stored at 4°C. Shortly before CE-MS analysis, the samples
411 were resuspended in 10 µl high-performance liquid chromatography grade water (HPLC-
412 H_2O).
413 *CE-MS analysis and data processing:* CE-MS experiments were conducted as previously
414 reported [42]. Briefly, a Beckman Coulter Proteome Lab PA800 capillary electrophoresis
415 system (Fullerton, CA) online coupled to a micrOTOF II MS (Bruker Daltonic, Bremen,
416 Germany) was used. The electro-ionization (ESI) sprayer (Agilent Technologies, Palo
417 Alto, CA) was grounded, and the ion spray interface potential was established to –4.5 kV.
418 Subsequently, data acquisition and MS acquisition methods were automatically measured
419 through the CE by contact-close-relays. Spectra were accrued every 3 seconds, over a
420 range of m/z 350 to 3000.
421 Mass spectral ion peaks signifying identical molecules at different charges were
422 deconvoluted into singles masses using MosaiquesVisu [43]. The subsequent peak lists
423 categorized each peptide according to its molecular mass (kDa), CE-migration time (min)
424 and signal intensity (amplitude). Due to the analytical variances of urine samples,
425 migration time and ion signal intensity (amplitude) were normalized using endogenous
426 "housekeeping" peptides, normally displaying a small difference between at least 90% of
427 all urine samples, as reported elsewhere [42]. Lastly, all detected peptides were deposited,
428 matched and annotated in a Microsoft SQL database [42]. Thus, further comparisons and
429 statistical analysis among both groups were performed.

Sequencing of peptides: Tandem mass spectrometry (MS/MS) analysis were conducted to retrieve the sequence information of the peptides, as previously described [42]. Briefly, MS/MS experiments were performed on a Dionex Ultimate 3000 RSLC nanoflow system (Dionex, Camberly, UK) coupled to an Orbitrap Velos MS instrument (Thermo Fisher Scientific). Thereafter, all resulting data files were evaluated by the use of SEQUEST (using Thermo Proteome Discoverer 1.2) without any enzyme specificity and searched beside the Swiss-Prot *Mus Musculus* database, as previously described[44].

Statistical analysis: For the identification of potential significant different urinary peptides, urine samples from both groups (wild type and *Tshz3*$^{+/lacZ}$) were compared. *P*-values were calculated according to the Wilcoxon Rank-Sum test. For multiple testing correction, the reported *p*-values were further adjusted via false discovery rate method described by Benjamini and Hochberg [45]. Only peptides with p-values less than 0.05 and detected in a frequency threshold of ≥70% in at least one of both groups were further considered as statistically significant. Statistical analysis was performed using Prism 7.05 (GraphPad Software, USA) and results considered significant at $P < 0.05$.

Data availability

The data that support the findings of this study are available from the corresponding author upon reasonable request. Raw data (FastQ files) from the sequencing experiment (triplicates from wild-type and *Tshz3*$^{+/lacZ}$ adult kidney) and raw abundance measurements for genes (read counts) for each sample are available from Gene Expression Omnibus (GEO) under accession GSE182010, which should be quoted in any manuscript discussing the data.

Ethics Statement

The animal study was reviewed and approved by "*Comité National de Réflexion Ethique sur l'Expérimentation Animale* 14" (ID numbers 57-07112012) and were in agreement with the European Communities Council Directive (2010/63/EU).

Acknowledgements

We appreciate feedback on the manuscript provided by Pierre L. Roubertoux and Adrian S. Woolf. Microscopy was performed at the imaging platform of the IBDM, supported by the ANR through the "Investments for the Future" program (France-BioImaging, ANR-10-INSB-04-01).

Funding

This work was supported by the European Union's Horizon 2020 research and innovation programme under the Marie Sklodowska-Curie grant agreement No 642937 (Scientific coordinator L.F), the French National Research Agency (ANR-17-CE16-0030-01 "TSHZ3inASD" project to L.F.), the Centre National de la Recherche Scientifique (CNRS), the Institut National pour la Recherche Médicale (INSERM) and Aix-Marseille University. I.S-M. and P.M. acknowledge financial support from the European Union's Horizon 2020 research and innovation PhD programme under the Marie Sklodowska-Curie grant agreement No 642937.

Competing Financial Interests

The authors declare no competing financial interests or potential conflicts of interest.

References

1. Schedl, A. Renal abnormalities and their developmental origin. *Nat Rev Genet* **8**, 791-802 (2007).
2. Chang, C.P. *et al.* Calcineurin is required in urinary tract mesenchyme for the development of the pyeloureteral peristaltic machinery. *J Clin Invest* **113**, 1051-8 (2004).
3. Klein, J. *et al.* Congenital ureteropelvic junction obstruction: human disease and animal models. *International Journal of Experimental Pathology* **92**, 168-92 (2011).
4. Caubit, X. *et al.* TSHZ3 deletion causes an autism syndrome and defects in cortical projection neurons. *Nat Genet* **48**, 1359-1369 (2016).
5. Caubit, X. *et al.* Teashirt 3 is necessary for ureteral smooth muscle differentiation downstream of SHH and BMP4. *Development* **135**, 3301-10 (2008).
6. Martin, E. *et al.* TSHZ3 and SOX9 regulate the timing of smooth muscle cell differentiation in the ureter by reducing myocardin activity. *PLoS One* **8**, e63721 (2013).
7. Caubit, X. *et al.* Teashirt 3 regulates development of neurons involved in both respiratory rhythm and airflow control. *J Neurosci* **30**, 9465-76 (2010).
8. Karaiskos, N. *et al.* A Single-Cell Transcriptome Atlas of the Mouse Glomerulus. *Journal of the American Society of Nephrology : JASN* **29**, 2060-2068 (2018).
9. Park, J. *et al.* Single-cell transcriptomics of the mouse kidney reveals potential cellular targets of kidney disease. *Science* **360**, 758-763 (2018).
10. Liu, J. *et al.* Cell-specific translational profiling in acute kidney injury. *The Journal of clinical investigation* **124**, 1242-54 (2014).
11. Mootha, V.K. *et al.* PGC-1alpha-responsive genes involved in oxidative phosphorylation are coordinately downregulated in human diabetes. *Nature Genetics* **34**, 267-73 (2003).
12. Subramanian, A. *et al.* Gene set enrichment analysis: a knowledge-based approach for interpreting genome-wide expression profiles. *Proceedings of the National Academy of Sciences of the United States of America* **102**, 15545-50 (2005).
13. Chen, E.Y. *et al.* Enrichr: interactive and collaborative HTML5 gene list enrichment analysis tool. *BMC Bioinformatics* **14**, 128 (2013).
14. Rubtsova, K., Rubtsov, A.V., van Dyk, L.F., Kappler, J.W. & Marrack, P. T-box transcription factor T-bet, a key player in a unique type of B-cell activation essential for effective viral clearance. *Proceedings of the National Academy of Sciences of the United States of America* **110**, E3216-24 (2013).
15. Good, D.M. *et al.* Naturally occurring human urinary peptides for use in diagnosis of chronic kidney disease. *Mol Cell Proteomics* **9**, 2424-37 (2010).
16. Caubit, X. *et al.* TSHZ3 deletion causes an autism syndrome and defects in cortical projection neurons. *Nature Genetics* **48**, 1359-1369 (2016).
17. Savige, J. *et al.* Thin basement membrane nephropathy. *Kidney Int* **64**, 1169-78 (2003).
18. Dimke, H., Maezawa, Y. & Quaggin, S.E. Crosstalk in glomerular injury and repair. *Curr Opin Nephrol Hypertens* **24**, 231-8 (2015).
19. Magalhaes, P. *et al.* Association of kidney fibrosis with urinary peptides: a path towards non-invasive liquid biopsies? *Sci Rep* **7**, 16915 (2017).

20. Wei, R. *et al.* Alterations in urinary collagen peptides in lupus nephritis subjects correlate with renal dysfunction and renal histopathology. *Nephrol Dial Transplant* **32**, 1468-1477 (2017).
21. Klein, J. *et al.* Urinary peptidomics provides a noninvasive humanized readout of diabetic nephropathy in mice. *Kidney Int* **90**, 1045-1055 (2016).
22. Mudge, J.M. *et al.* Dynamic instability of the major urinary protein gene family revealed by genomic and phenotypic comparisons between C57 and 129 strain mice. *Genome Biol* **9**, R91 (2008).
23. Thoss, M. *et al.* Regulation of volatile and non-volatile pheromone attractants depends upon male social status. *Sci Rep* **9**, 489 (2019).
24. Gallagher, J.C. & Seligson, D. Significance of abnormally low blood urea levels. *N Engl J Med* **266**, 492-5 (1962).
25. Lum, G. & Leal-Khouri, S. Significance of low serum urea nitrogen concentrations. *Clin Chem* **35**, 639-40 (1989).
26. de Baaij, J.H., Hoenderop, J.G. & Bindels, R.J. Regulation of magnesium balance: lessons learned from human genetic disease. *Clin Kidney J* **5**, i15-i24 (2012).
27. Liu, S. & Quarles, L.D. How fibroblast growth factor 23 works. *J Am Soc Nephrol* **18**, 1637-47 (2007).
28. Lederer, E. Regulation of serum phosphate. *J Physiol* **592**, 3985-95 (2014).
29. Clothier, J. & Absoud, M. Autism spectrum disorder and kidney disease. *Pediatr Nephrol* (2020).
30. Meyer, E. *et al.* Mutations in the histone methyltransferase gene KMT2B cause complex early-onset dystonia. *Nat Genet* **49**, 223-237 (2017).
31. Wu, L.L., Mao, S.S., Lin, X., Yang, R.W. & Zhu, Z.W. Evaluation of Whole Blood Trace Element Levels in Chinese Children with Autism Spectrum Disorder. *Biol Trace Elem Res* **191**, 269-275 (2019).
32. Saldanha Tschinkel, P.F., Bjorklund, G., Conon, L.Z.Z., Chirumbolo, S. & Nascimento, V.A. Plasma concentrations of the trace elements copper, zinc and selenium in Brazilian children with autism spectrum disorder. *Biomed Pharmacother* **106**, 605-609 (2018).
33. Strambi, M. *et al.* Magnesium profile in autism. *Biol Trace Elem Res* **109**, 97-104 (2006).
34. Guo, M. *et al.* Vitamin and mineral status of children with autism spectrum disorder in Hainan Province of China: associations with symptoms. *Nutr Neurosci* **23**, 803-810 (2020).
35. Subramanian, A. *et al.* Gene set enrichment analysis: a knowledge-based approach for interpreting genome-wide expression profiles. *Proc Natl Acad Sci U S A* **102**, 15545-50 (2005).
36. Mootha, V.K. *et al.* PGC-1alpha-responsive genes involved in oxidative phosphorylation are coordinately downregulated in human diabetes. *Nat Genet* **34**, 267-73 (2003).
37. Livak, K.J. & Schmittgen, T.D. Analysis of relative gene expression data using real-time quantitative PCR and the 2(-Delta Delta C(T)) Method. *Methods* **25**, 402-8 (2001).
38. Relaix, F., Rocancourt, D., Mansouri, A. & Buckingham, M. Divergent functions of murine Pax3 and Pax7 in limb muscle development. *Genes Dev* **18**, 1088-105 (2004).
39. Schneider, C.A., Rasband, W.S. & Eliceiri, K.W. NIH Image to ImageJ: 25 years of image analysis. *Nature methods* **9**, 671-5 (2012).

40. van den Berg, J.G., van den Bergh Weerman, M.A., Assmann, K.J., Weening, J.J. & Florquin, S. Podocyte foot process effacement is not correlated with the level of proteinuria in human glomerulopathies. *Kidney Int* **66**, 1901-6 (2004).
41. Deegens, J.K. *et al.* Podocyte foot process effacement as a diagnostic tool in focal segmental glomerulosclerosis. *Kidney Int* **74**, 1568-76 (2008).
42. von zur Muhlen, C. *et al.* Urine proteome analysis reflects atherosclerotic disease in an ApoE-/- mouse model and allows the discovery of new candidate biomarkers in mouse and human atherosclerosis. *Molecular & cellular proteomics : MCP* **11**, M111 013847 (2012).
43. Neuhoff, N. *et al.* Mass spectrometry for the detection of differentially expressed proteins: a comparison of surface-enhanced laser desorption/ionization and capillary electrophoresis/mass spectrometry. *Rapid communications in mass spectrometry : RCM* **18**, 149-56 (2004).
44. Nkuipou-Kenfack, E. *et al.* The use of urinary proteomics in the assessment of suitability of mouse models for ageing. *PLoS One* **12**, e0166875 (2017).
45. Benjamini, Y. & Hochberg, Y. Controlling the False Discovery Rate: A Practical and Powerful Approach to Multiple Testing. *Journal of the Royal Statistical Society. Series B (Methodological)* **57**, 289-300 (1995).

1 **Figures**

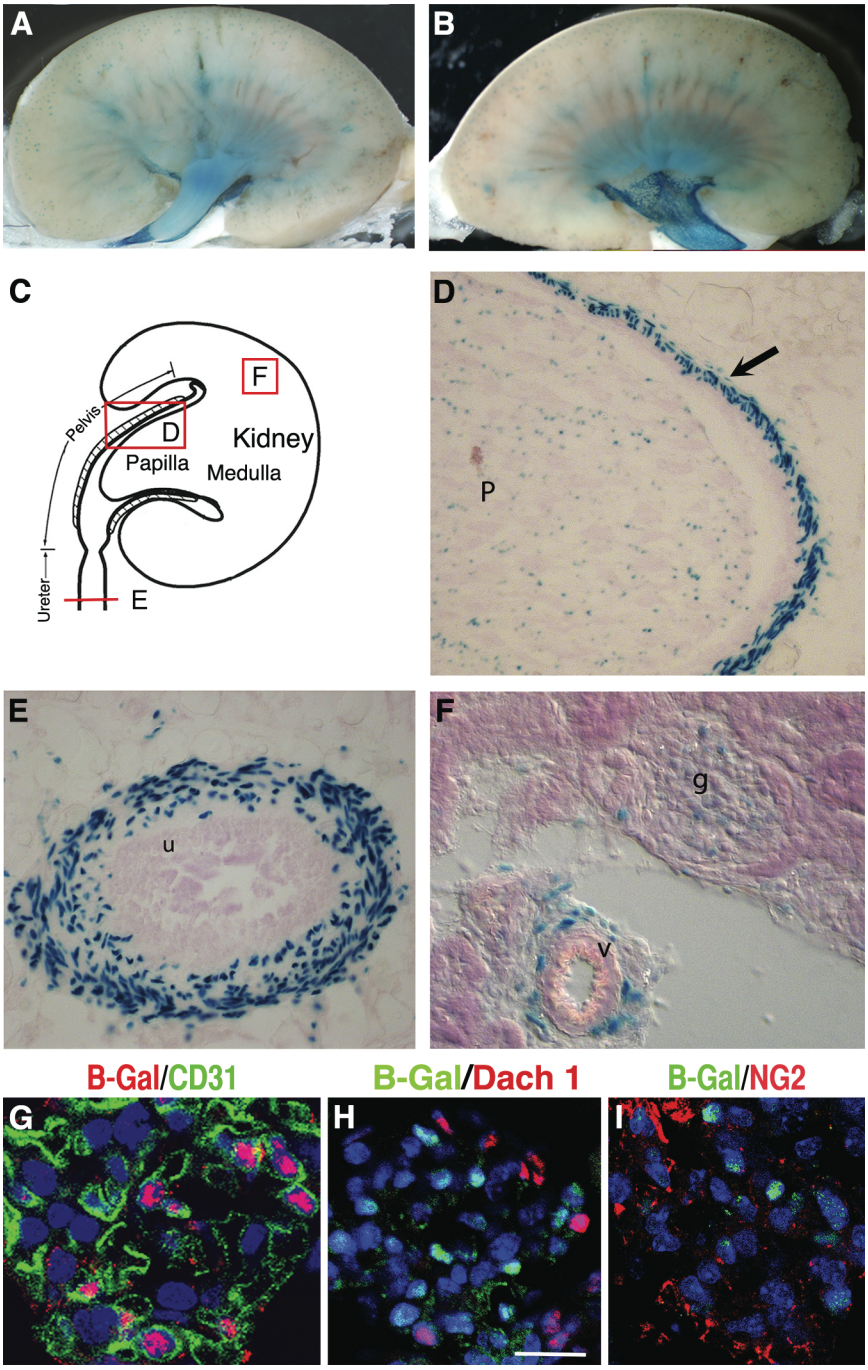

2

3 **Figure 1. Distribution of Xgal-positive cells in *Tshz3*$^{+/lacZ}$ adult renal tract.** (A, B) The two
4 halves of the same adult kidney stained with X-Gal. (C) Cartoon showing the section sites and
5 planes for D, E and F. (D-F) Xgal-Positive cells were found in papilla (p) and smooth muscle
6 present in the pelvic region (arrow) (D), in the mesenchymal part of the ureter (E), in the
7 glomeruli (g) and in close proximity to blood vessel (v) (F). (G-I) In glomeruli, TSHZ3 (ß-Gal)
8 is detected in CD31+ glomerular endothelial cells (G) but not in DACH1+ podocytes (H) or in
9 NG2+ mesangial cells (I); scale bar, in G-I, 20 µm. B-Gal, Beta-Galactosidase; u: urothelium.

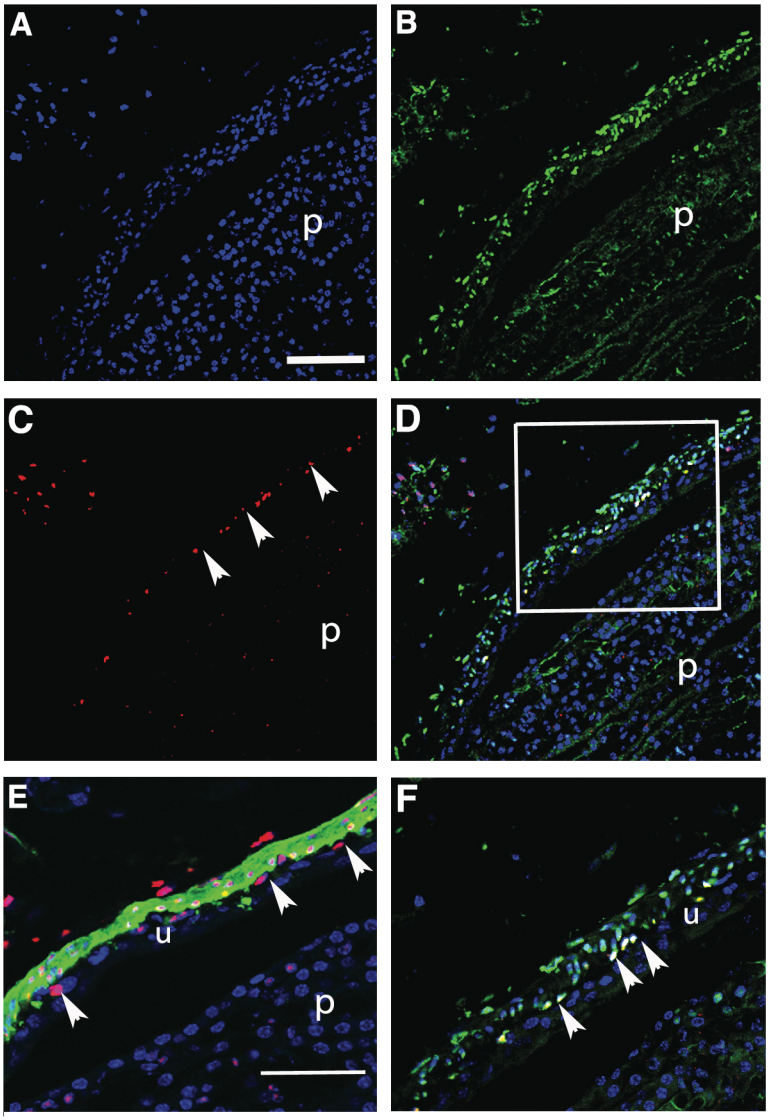

Figure 2. Characterization of β-galactosidase-positive cells in the pelvic region of *Tshz3*$^{+/lacZ}$ adult kidney. (A-D) Comparative expression of ß-galactosidase (green) and Dachshund 1 (red) in the pelvic region. (F) Close up of the region boxed in D. Merge image (D, F) shows that a subset of βgal+ cells expresses DACH1 (arrowheads in C and F). These cells represent a cell layer in a sub urothelial position. (E) Double immunostaining for βgalactosidase (red) and smooth muscle actin (green) indicates that βgal expression is found in SMA expressing cells. Some βgal+ cells adjacent to the urothelium do not express SMA (arrowheads in E). P: papilla, u: urothelium. Scale bars, in A, 100µm; in E, 50µm.

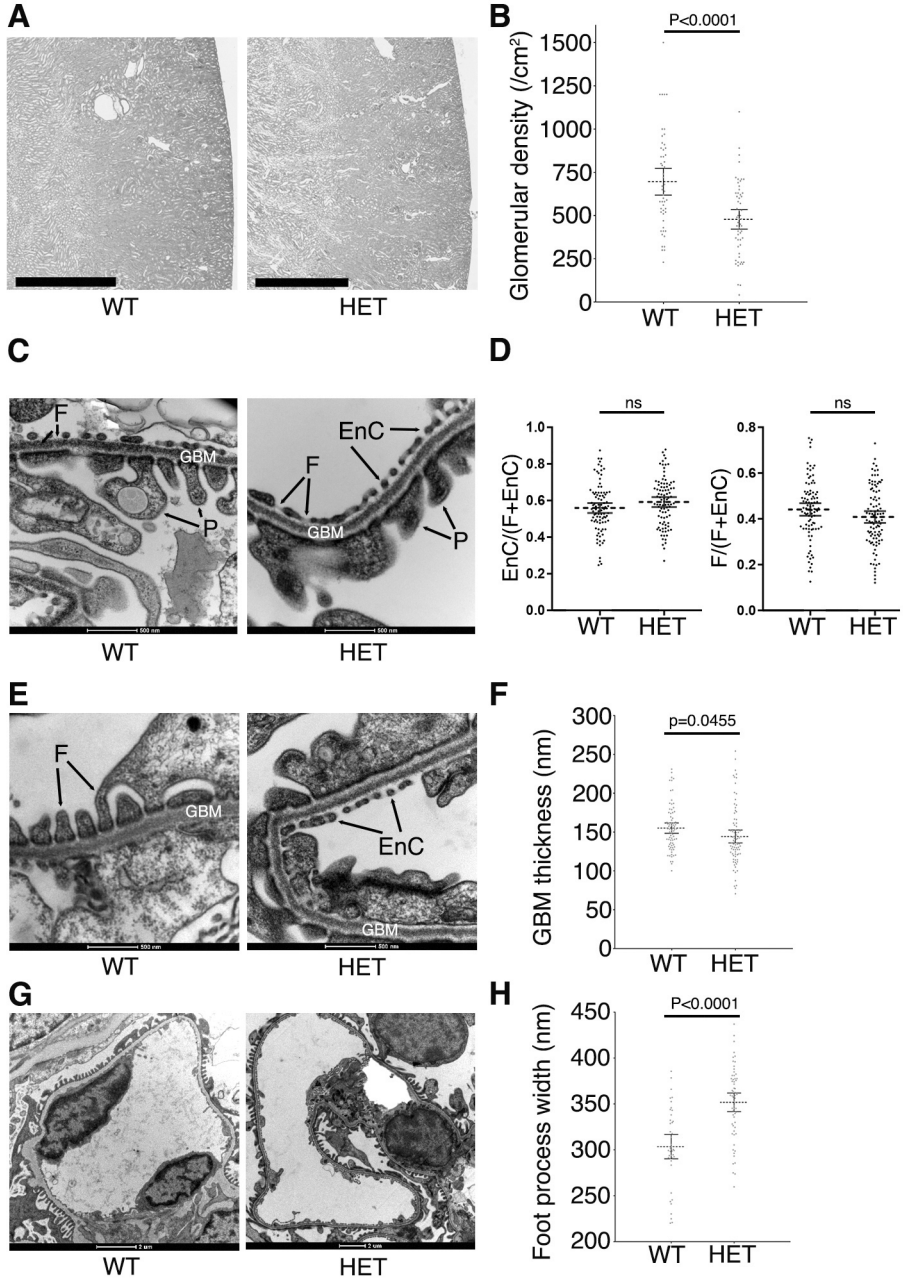

Figure 3: Reduced glomerular density, glomerular basement membrane thinning and foot process effacement in heterozygous *Tshz3*$^{lacZ/+}$ mice. (A) Representative images of haematoxylin and eosin-stained sections of WT and *Tshz3*$^{+/lacZ}$ adult kidneys at post-natal day 60. Scale bar 1mm. (B) The graph shows the significant (P<0.0001) reduction of the glomerular density in heterozygous *Tshz3*$^{lacZ/+}$ (471 ± 0.29 /cm^2, 48 sections from 3 kidneys) compare to wild-type kidney (695 ± 0.38 /cm^2, 41 sections from 3 kidneys). (C, E, G) Representative TEM images of wild type and *Tshz3*$^{+/lacZ}$ adult kidneys. (D, F, H) TEM morphometric analysis. (C) TEM: No abnormalities in endothelial cell fenestration are observe in *Tshz3*$^{+/lacZ}$ mice. Scale bar, 500nm. (D) Morphometric analysis of the fenestration reveals no significant difference between WT and *Tshz3*$^{+/lacZ}$ mice. (E) TEM: *Tshz3*$^{+/lacZ}$ kidney shows a reduction of the

thickness of the GBM in *Tshz3*$^{lacZ/+}$ compared to WT. Scale bar, 500nm. (F) Morphometric analysis reveals a significant reduction (P<0.0455) of the thickness of the GBM in *Tshz3*$^{lacZ/+}$ (144.2 ± 4.2 nm, 84 sections from 3 kidneys) compare to wild-type (155.1 ± 3.32 nm, 78 sections from 3 kidneys). (G) TEM: illustrating increased foot process effacement in *Tshz3*$^{lacZ/+}$ compared to WT mice. Scale bar, 2µm. (H) Foot process width in WT (303.4 ± 6.57 nm, 42 sections from 7 kidneys) is significantly lower (P<0.0001) compared to *Tshz3*$^{lacZ/+}$ (351.7 ± 5.03 nm, 61 sections from 9 kidneys) mice. Data are shown as mean and its 95% CI. EnC, endothelial cell cytoplasm; F, endothelial fenestration; GBM, glomerular basement membrane; HET, hererozygous; P, podocyte foot process; SD, standard deviation; WT, wild type.

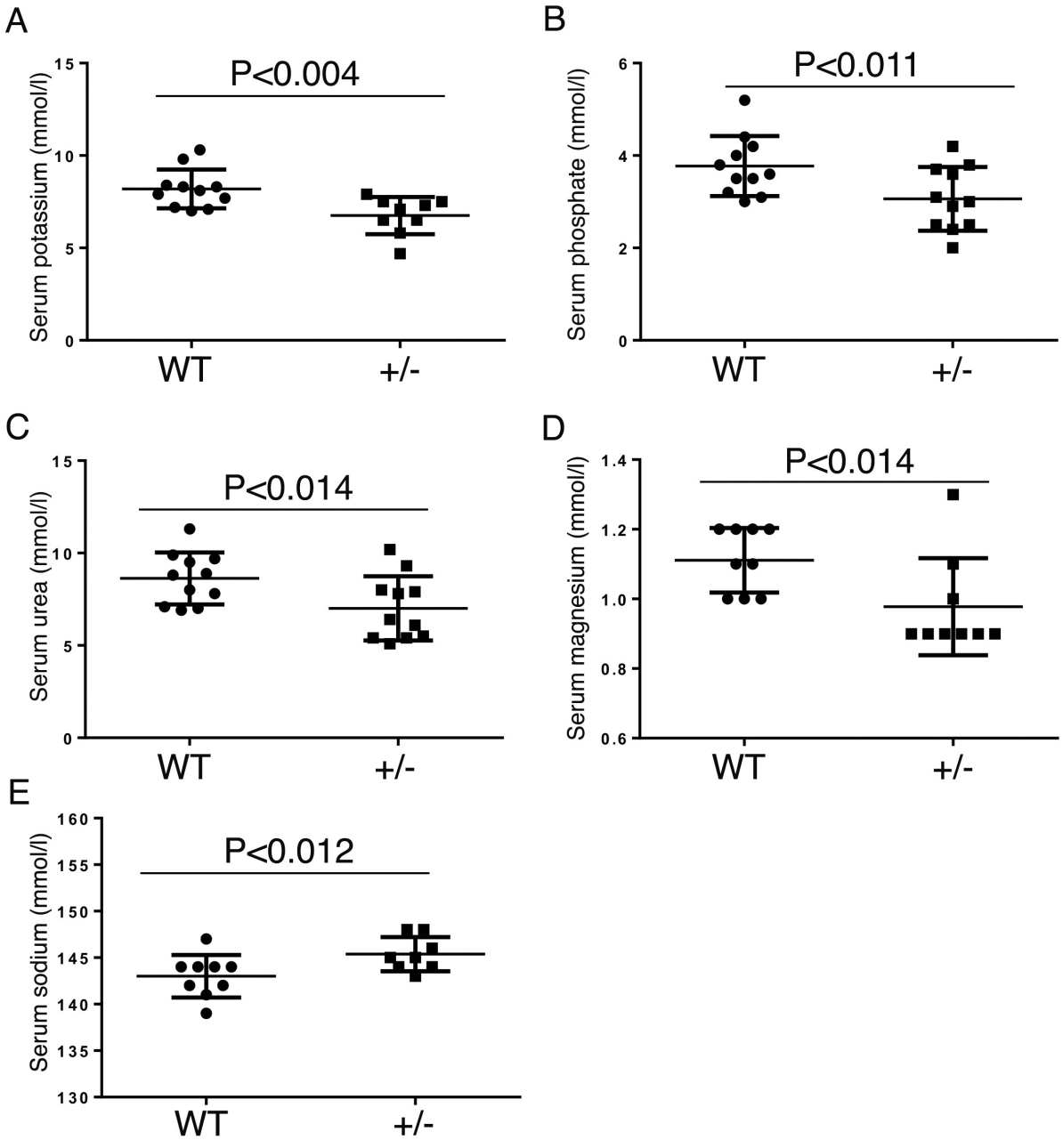

Figure 4. **Differences in serum biochemical parameters between control and *Tshz3*$^{lacZ/+}$ mice**. Plasma concentration of potassium (A), phosphates (B), urea (C), magnesium (D) and sodium (E). Data are represented as means ± SEM. Statistically significant difference from control at *p<0.02; **p<0.004. WT, wild type; +/-, *Tshz3*$^{+/lacZ}$

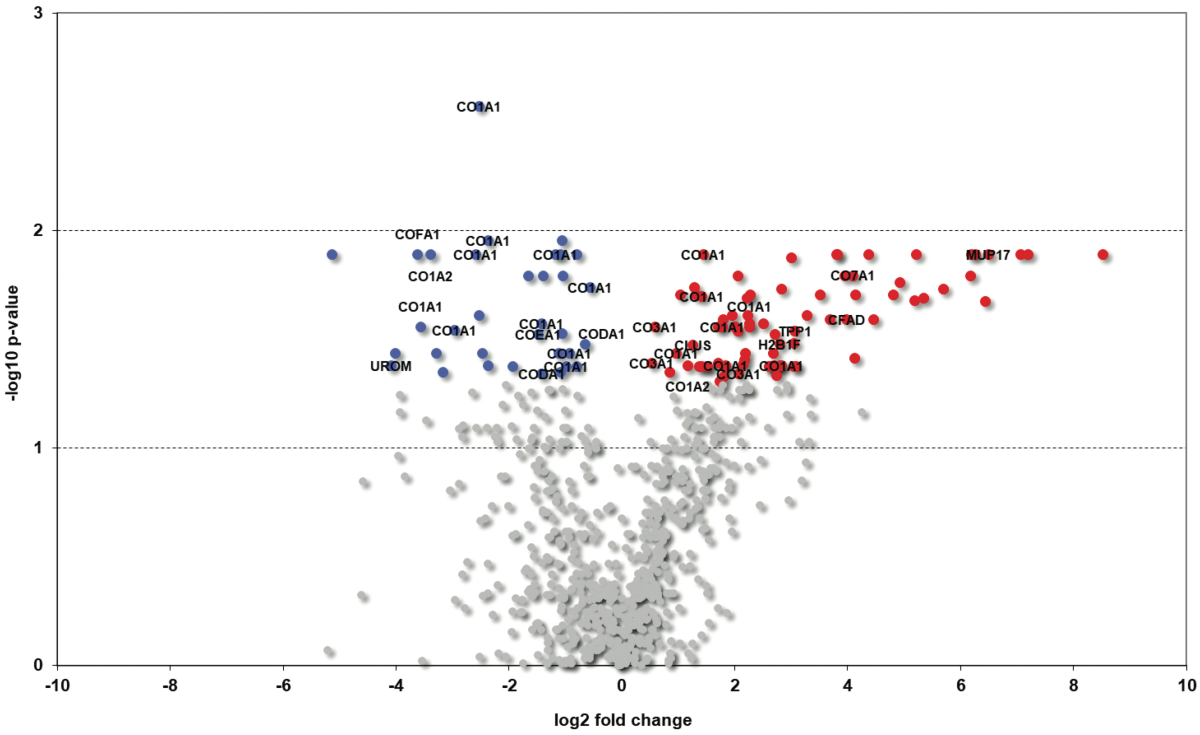

Figure 5. Urinary peptides displaying differential abundance in *Tshz3*$^{+/LacZ}$ mice. The volcano plot of quantified proteins revealed that 115 peptides (red and blue dots) show a significant change (p-value <0.05) in *Tshz3*$^{+/lacZ}$ compared to control mice. However, for 33 of these peptides we were able to find a sequence (labeled ones; see **Table 1i**). The grey dots are peptides that have not a significant change (p-value >0.05).